Interpretation of Pressuremeter Test by Finite Element Method

Author 1

- Yi Rui, PhD
- Centre for Smart Infrastructure & Construction, Department of Engineering, University of Cambridge, UK.

Author 2

- Mei Yin, PhD
- Centre for Smart Infrastructure & Construction, Department of Engineering, University of Cambridge, UK.

Corresponding Author

- Mei Yin,PhD
- Department of Engineering, Trumpington Street, Cambridge, CB2 1PZ, UK
  myin0915@gmail.com

Abstract

A pressuremeter test is a useful tool to explore geomechanical properties by comparing the in-situ measured stress-strain relationship with proposed soil behaviour. In this paper, a coupled hydro-mechanical finite element model is developed to interpret pressuremeter test data, considering nonlinear elasticity, tensile fracturing and consolidation of soil. The 1D finite element model reduced the total number of elements and hence saved computational time without losing accuracy. It is found that tensile fracturing plays an important role for the cohesive clay, which would lead to overestimation of the stiffness and strength if the tensile failure is not considered. In addition, consolidation needs to be considered when the permeability coefficient is between $10^{-10}\mathrm{m}/s$ and $10^{-8}\mathrm{m}/s$, and the errors of derived stiffness constant and friction angle can reach a maximum of 21% and 35.5% respectively if neglecting consolidation.

Keywords

Pressuremeter test, finite element, tensile fracturing, consolidation

List of notation

α stiffness constant

β exponent of elasticity

p pore pressure

k permeability coefficient

u displacement of soil

σ'_t tensile strength

σ'_3 minor principal effective stress

σ'_r radial effective stress

σ'_θ circumferential effective stress

γ_w unit weight of water

K_w bulk modulus of water

ε_{pt} tensile plastic strain

1 Introduction

The pressuremeter test is a widely used in-situ test to achieve quick and easy measurement of the stress-strain relationship of soil. By comparing this stress-strain relationship with proposed soil behaviour, some geomechanical parameters can be determined. It is common sense that the pressuremeter test can provide accurate estimates of soil properties due to its little soil disturbance in situ. However, in practice, it has been found that there are still some uncertainties about the interpretation of test data due to the complexity of soil physical properties.

In general, interpreting pressuremeter test involve fitting curves to the test data (Clarke 1995; Schnaid et al. 2000). This interpreting approach rely either on empirical correlations, or on solving the boundary problem. Due to the pressuremeter test normally being performed over a short period of time, a number of analytical models have been proposed to interpret the pressuremeter test in clay under undrained conditions (Gibson and Anderson, 1961; Wroth, 1982; Jefferies, 1988; Bolton and Whittle, 1999; Cunha 1994; Cunha 1996). All these studies simplified the pressuremeter test as an undrained cylindrical cavity expansion in elastic/perfectly plastic clay. Unlike in clay, interpreting the results of a pressuremeter test in sands or rocks with a high permeability coefficient, the approaches consider the volume change in drained conditions (Hughes et al., 1977; Houlsby and Withers, 1988; Withers et al., 1989; Yu and Houlsby, 1991; Yu, 2000; Mo et al., 2014). These analytical methods bring convenience in curve-fitting analysis when interpreting pressuremeter test data due to the explicit formulation and hence quick calculation. Numerical method has recently become an effective and widely-used mathematical tool for modeling more complicated soil behaviour in pressuremeter test (Yeung and Carter, 1990; Houlsby and Carter, 1993; Ajalloeian and Yu, 1998; Sánchez et al., 2014; Isik et al., 2015). It has been shown that numerical analysis can obtain more accurate results compared to the analytical method, due to its capacity and flexibility for implementing complex constitutive models and boundary conditions to simulate the complicated soil behaviours. However, the degree of complexity of these numerical models inhibits the curve-fitting analysis into general purpose numerical codes, thus restricting their usefulness in engineering practice. (Emami and Yasrobi, 2014). In addition, most of these studies neglect the effects of tensile fracturing and consolidation on soil behaviour in this particular geotechnical problem. For some soils with medium permeability, the soil is partially drained, and hence lie somewhere between the perfectly drained and undrained conditions. For some cohesive materials, tensile failure may happen before friction failure during the pressurmeter test.

This paper depicts numerical modelling based on the 1D finite element (FE) method, purposely designed for pressuremeter test. This FE modelling allows for considering complex constitutive models and capturing complete soil response with different geomechanical parameters, including nonlinear elasticity, permeability coefficient and tensile strength. The comparison of test results with the numerical reference framework indicates a method to determine the geomechanical parameters of soil, which will help understand the mechanisms of pressuremeter test. Due to the simplified geometry, the curve-fitting analysis can be easily incorporated for industry application. Therefore, this 1D finite element modelling can be a framework for the interpretation of pressuremeter test.

2 Finite Element for coupled hydro-mechanical process

During the pressuremeter test, a rubber membrane of the pressuremeter is expanded to exert horizontal pressure on the wall of the test cavity. The membrane expands at the constant strain rate, generally from 0.1% to 1% per minute in typical tests. The successive variation of cavity pressure with cavity strain is monitored and then compared with those obtained from numerical analysis to determine the geomechanical parameters. To simulate such a geomechanical process, the pressuremeter test is simplified as a time-dependent cylindrical cavity expansion in an elastic/plastic porous medium (soil) coupled with the dissipation of excess pore pressure. Some assumptions have been adopted based on the theory of continuum mechanics to develop the coupled hydro-mechanical model for deformable porous geological media:

(1) The soil is treated as a fully saturated medium.
(2) The seepage flow of pore water follows Darcy's law, and the inertia is ignored.
(3) The membrane is assumed to be long enough to ensure that a cylindrical cavity is formed and this cavity expands and contracts in plain strain condition.
(4) Considering the axial symmetry of geometry, the plane strain model can be further simplified to a 1D problem, to reduce the computational load without losing accuracy.

A finite element model in 1D axisymmetric space is built as shown schematically in Figure 1. All the FE analysis discussed in this paper is based on this model. This soil layer is located at the centre of the pressuremeter membrane. The initial cavity radius is 0.045m, same with the radius of pressuremeter membrane, but this radius would increase with the cavity expansion. The right boundary lies in the far field, 10m away from cavity center, to avoid boundary effects. Vertical movement is restrained, and hence the 1D model has only two degrees of freedom: displacement in radial direction and pore water pressure. The assumed initial condition includes the hydrostatic state of the soil and pore pressure. There are 120 quadratic elements generated in total, and the mesh near the pressuremeter is relatively finer than that in the far field. In order to simulate the large soil deformation in this test, the calculation mesh is modified in each stage. At the end of each stage, the displacement increment of each node will be added to the coordinates, so that the new family of radius is updated based on the deformed meshes from the previous stage.

Figure 1. Sketch of the numerical model to simulate a pressuremeter test

In the context of the theory of mixtures, the saturated porous medium is viewed as a mixed continuum of two independent overlapping phases. Its conservation equation can be obtained according to the principles of continuum mechanics, as shown in Figure 2.

Figure 2. Soil stress and pore flow velocity in axisymmetric problem

(1) Axisymmetric elastic equations:

If momentum can be neglected, the stress equilibrium for axisymmetric problem can be written as follows:

$$\frac{\partial \sigma_r'}{\partial r} + \frac{\sigma_r' - \sigma_\theta'}{r} + \frac{\partial p}{\partial r} = 0 \quad (1)$$

where σ_r' is the radial effective stress, σ_θ' is the circumferential effective stress, p is the pore pressure, r is the radial coordinate.

The strain components for axisymmetric deformation are defined as follows:

$$\varepsilon_r = \frac{\partial u_r}{\partial r} \tag{2}$$

$$\varepsilon_\theta = \frac{u_r}{r} \tag{3}$$

where u_r is the displacement in radial direction, ε_r is the radial strain and ε_θ is the circumferential strain.

Hence, the volumetric strain can be written by:

$$\varepsilon_{vol} = \varepsilon_r + \varepsilon_\theta = \frac{\partial u_r}{\partial r} + \frac{u_r}{r} \tag{4}$$

The porous medium is assumed to be isotropic. If the shear modulus is assumed, the elastic constitutive equation can be expressed in terms of stress and strain increments:

$$d\sigma'_r = \frac{2G\nu}{1-2\nu} d\varepsilon_{vol} + 2\theta d\varepsilon_r \tag{5}$$

$$d\sigma'_\theta = \frac{2G\nu}{1-2\nu} d\varepsilon_{vol} + 2G d\varepsilon_\theta \tag{6}$$

where G is shear modulus and ν is Poisson's ratio.

(2) Axisymmetric seepage equations:

In this study, the flow of pore water obeys Darcy's law. Hence, the flow velocity q_r can be written as:

$$q_r = \frac{k}{\gamma_w} \frac{\partial p}{\partial r} \tag{7}$$

where k is the permeability coefficient (m/s), γ_w is the unit weight of water.

The mass conservation between volumetric strain and water drainage leads to the storage equation:

$$\frac{1}{r} \frac{\partial}{\partial r}(r q_r) + \frac{d}{dt} \varepsilon_{vol} - \frac{n}{K_w} \frac{dp}{dt} = 0 \tag{8}$$

where n is the porosity and K_w is the bulk modulus of pore water.

Taking Equations (4) and (7) into Equation (8):

$$\frac{k}{\gamma_w} \frac{\partial^2 p}{\partial r^2} + \frac{k}{\gamma_w \cdot r} \frac{\partial p}{\partial r} + \frac{d}{dt}\left(\frac{\partial u_r}{\partial r} + \frac{u_r}{r}\right) - \frac{n}{K_w} \frac{dp}{dt} = 0 \tag{9}$$

The balance of relations, listed above, characterises the fundamental physical properties of matter independently of its specific material properties. However, in the pressuremeter test, the response of soil to similar interactions with cavity expansion differs for various geomaterials. Thus, constitutive relations have to be defined to characterize specific mechanical behaviour. Bolton and Whittle (1999) indicate that the application of linear elastic analysis to a non-linear elastic problem will give a wrong interpretation of the distribution of stresses and strains in the pressuremeter test. Hence, a power law function is applied to simulate the stiffness degradation of the soil, which was first proposed by Gunn (1992) and Bolton et al. (1993). The stress-strain relationship is expressed as:

$$\tau = \alpha\gamma^{\beta} \qquad (10)$$

Where τ is shear stress, γ is the shear strain, α is the stiffness constant and β is the exponent of elasticity.

In this finite element model, soil is defined as a elastic/perfectly plastic material. The Mohr-Coulomb model is applied to define the shear strength of the soils at different effective stresses. Except for shear failure, tensile fracturing is one of the most important processes in the pressuremeter test. It is a process of initiation and propagation of a thin physical separation when the soil effective stress drops below the tensile strength. .

The tension yield function is used, and can be written in the form of the minor principal effective stress:

$$f^{t} = \sigma'_{\mathrm{t}} - \sigma'_{3} \qquad (11)$$

where σ'_t is the tensile strength and σ'_3 is the minor principal effective stress. During the process of cavity expansion in clay, because of the increasing difference between the radial and circumferential stress imposed by the applied pressure, the soil is sheared. The circumferential stress becomes the minor principal effective stress. If equation (11) is satisfied, tensile fracturing occurs, as shown in Figure 3.

Figure 3. Mechanisms of tensile fracturing in undrained conditions (after Mitchell and Soga, 2005)

Tensile failure happens when the tensile failure criterion is violated. The material still behaves as a continuum after the occurrence of tensile failure. In addition, the tensile potential function is assumed to follow the associated flow rule. Under conditions of tensile failure, the tensile strength is assumed to soften gradually rather than diminishing immediately. The softening law is shown in Figure 4b, where the tensile strength decreases from σ'_{t} to zero when the tensile plastic strain ε_{pt} increases from 0 to 0.01 (Ng 2009). The complete yield surface, incorporating shear and tension yield functions, is shown in Figure 4a.

Figure 4. (a) complete yield surface (b) softening law of tensile strength

3 Drained and undrained analysis

Based on the formulations discussed above, an in-house finite element program was written. This is a procedural finite-element code using generic programming. In order to validate the finite element model, two different series of case studies were conducted, including drained and undrained analysis.

To interpret the sand strength in the pressuremeter test, Yu and Houlsby (1991) derived a widely accepted analytical solution. This solution is based on Cavity Expansion Theory, using the logarithmic strain and Mohr-Coulomb model parameters. Figure 5 compares Yu and Houlsby's closed-form solution and data generated by linear elastic finite element drained analysis with different values of shear modulus. All parameters are as listed in Table 1 (drained analysis). In this analysis, the pore pressure on every nodes is fixed as 0, which eliminate the effect of pore pressure on effective stress. Displacement boundary conditions will be applied on the left boundary abutting the instrument to simulate the cavity expansion, as shown in Figure 1. The cavity strain increases from 0 to 5%. The initial effective stress is set as 100kPa. 3 case studies with shear modulus of 50 MPa, 100 MPa and 200 MPa were performed respectively. Yu's solution matches the FE-generated curve outstandingly well, which implies that both the elastic/plastic deformation and the large strain formulation have been properly taken into account.

Table 1 Soil parameters for drained/undrained analysis

Figure 5. Cavity expansion curve from numerical drained analysis and analytical solution

Undrained analysis can be performed in terms of either effective or total stresses. During the loading and yielding process, a significant amount of excess pore pressure would be developed. This excess pore pressure would lead to a change of the effective stress and therefore influence the shear strength of the soil. Hence, the success of such analysis relies on whether the adopted constitutive model can correctly predict the development of effective stress and pore water pressure. If elastic perfect plastic model used, the prediction of pore water pressure in the pre-failure regime may be away from the real situation. Bolton and Whittle (1999) derived the undrained shear strength of clay in the pressuremeter test, assuming that the ground response to loading/unloading is non-linear elastic/perfectly plastic. A non-linear elastic/perfectly plastic undrained analysis was carried out using the proposed model in this paper. The hydro-mechanical coupling model can be used to carry out an effective stress analysis of pressuremeter test when the permeability coefficient k is set as 0. Figure 6 shows the comparison of Bolton and Whittle's analytical solution and the results of the finite element simulation with different stiffness constants. All parameters are as listed in Table 1 (undrained analysis). Three case studies with different stiffness constant were performed. The numerical result matches the analytical solution, which indicates that the nonlinear elasticity model has been correctly implemented, which provides some confidence in using the FE model.

Figure 6. Cavity expansion curve from numerical undrained analysis and analytical solution

4 Effects of tensile fracturing

Ng (2009) conducted tests of cavity expansion to simulate a pressuremeter test and tensile fracturing in cement bentonite. The borehole was modelled by a cylindrical specimen with an inner central cylindrical cavity. A rubber membrane was inserted into the inner cylindrical cavity of the specimen so that the injected water could apply pressure to the specimen's cavity through membrane expansion. Tests were performed in undrained conditions as the permeability of cement bentonite is very low. One of the test data is used as reference for comparison with FE analysis in this paper. The purpose of this paper is to demonstrate the effects of tensile fracturing and consolidation. Only the loading stage of test is simulated.

Two series of FE analyses were performed. The first is shear analysis using the Mohr-Coulomb model, which only considers the shear failure. The second is tensile/shear analysis which considers both shear failure and tensile failure. All the parameters used in the FE analysis are listed in Table 2. The calculation was divided into 250 steps. In each step the cavity strain increased 0.02%, as a boundary condition applied on the left boundary. Permeability coefficient was 0 m/s. The cohesion and the friction angle were 235 kPa and 20°, according to the undrained triaxial test results of bentonite material (Joshi et al., 2008). The dilation angle and tensile strength were 0° and 65 kPa, based on the results of the Brazilian tests (Ng, 2009). The test data from Ng (2009) was used to calibrate the stiffness constant and exponent of elasticity, as shown in Figure 7.

Table 2 Soil parameters for shear and tensile/shear analysis

The FE results are shown in Figure 7. With the same stiffness constant of 8 MPa, the cavity pressure is 10% larger for the tensile/shear analysis than for the shear analysis when the cavity strain is about 5%. In order to fit the test data with the same degree of accuracy, the stiffness constant needs to be reduced to 6.5 MPa for the tensile/shear analysis. Hence, it is concluded that failing to consider tensile fracturing leads to an underestimate of the cavity pressure and hence overestimate of the stiffness.

Figure 7. Cavity expansion curve for shear and tensile/shear analysis

The effective stress paths are presented in Figure 8, in which the change of effective radial stress with effective circumferential stress at the cavity wall is plotted. For the shear analysis, the increase in radial stress has a linear relationship with the decrease in circumferential stress until the shear stress reaches the yield surface. However, in the tensile/shear analysis, this turning point happens much earlier, when the effective circumferential stress is reduced to the tensile strength of -65 kPa. Due to tensile strength would soften gradually, it is shown that the effective circumferential stress increases a little after tensile failure. Between the case of shear analysis with $\alpha = 8\ \mathrm{MPa}$ and the tensile/shear analysis with $\alpha = 6.5\ \mathrm{MPa}$, there is a marked difference in effective radial stress and circumferential stress. However, the difference in the cavity pressure at 5% strain is negligible, as shown in Figure 7, which indicates that considering tensile fracturing produces a much lower estimate of excess pore pressure during the cavity expansion process. This is reasonable, because the tensile fracture can lead to relief of the excess pore pressure.

Figure 8. Stress path at the cavity wall

The above process can be plotted in the form of Mohr's circles, as shown in Figure 9. In the shear analysis, as shown in Figure 9(a), the diameter of the Mohr's circles continues to increase and the centre of the Mohr circle keeps constant, initially corresponding to the undrained condition. The Mohr's circles finally stop expanding when the Mohr-Coulomb shear failure criterion is violated, and the effective radial stress reaches 520 kPa. In the tensile/shear analysis, as shown in Figure 9(b) and 9(c), the soil undergoes tensile failure before reaching shear failure. After tensile failure, the centres of the Mohr's circles begin to move. The Mohr's circles finally reach the Mohr-Coulomb shear failure criterion with a much larger effective radial and circumferential stress than when tensile failure is not considered.

Figure 9. Mohr's circles at the cavity wall: (a) shear analysis ($\alpha = 8$Mpa); (b) tensile/shear analysis ($\alpha = 6.5$Mpa); (c) tensile/shear analysis ($\alpha = 8$Mpa)

In practice, the pressuremeter tests on low permeability soils are usually interpreted using total stress analysis, the undrained shear strength and elastic modulus can be estimated separately when other parameters are assumed. In this effective stress analysis, the cohesion and other parameters are assumed, as shown in Table 2, so that the stiffness constant or friction angle can be determined in each case study with different value of tensile strength. Figure 10 shows the derived stiffness constant and friction angle by interpreting data from Ng (2009), assuming that a stiffness constant of 6.5 MPa and a friction angle of 20° are the real values. It seems that a high tensile strength value used in the model leads to an overestimation of the stiffness constant and friction angle. When the tensile strength increases beyond 140 kPa, the estimated stiffness constant and friction angle reaches about 7.9 MPa and 38°, respectively. This case is close to the shear analysis, in which the stress reaches the shear failure criteria before tensile failure occurs. Therefore, it can be concluded that tensile fracturing plays an important role in the pressuremeter test, and choosing a suitable tensile strength is very important in interpreting test data.

The success of this tensile/shear analysis lies on the accurate prediction of tensile failure and subsequent shear failure. For non-cohesive soil, shear failure would happen before the effective circumferential stress drops below 0 kPa, and hence the tensile stress will no longer occur. Hence, the proposed effects of tensile fracturing on pressuremeter test data only applies for cohesive soil, especially with high cohesion and low tensile strength. This effects reduces with the decreases of soil cohesion, and tensile/shear analysis becomes completely unnecessary for non-cohesive soil.

Figure 10. Effect of tensile strength on soil stiffness and strength

5 Effects of consolidation

Normally, pressuremeter testing in clay is considered an undrained process, but in reality some consolidation occurs for soil with medium permeability. In this section, a series of finite element analyses were performed to assess the effects of consolidation on the derived parameters from the pressuremeter test. To avoid the coupled effects of tensile fracturing and consolidation, the parameters were based on the shear analysis, as listed in Table 2 (shear analysis). The calculation was also divided into 250 steps and the cavity strain increased 0.02% in each step. Duration of each step was 12 seconds, corresponding to a conventional cavity strain rate of 0.1%/min adopted in the self-boring pressuremeter test. Figure 11 shows the cavity pressure for different values of the permeability coefficient. Initially, the cavity pressure increases with increasing cavity strain, and all the cases coincide to a single curve. After the cavity strain increases over 1%, individual curves show different behaviour. With a permeability coefficient of $10^{-8}\ \mathrm{m/s}$, the cavity pressure reaches about 1610 kPa when the strain is about 5%. This is much higher than the case of $\mathrm{k} = 10^{-10}\mathrm{m/s}$, in which the highest cavity pressure is about 1450 kPa. In addition, the stress–strain curves for the cases of the undrained condition and $\mathrm{k} = 10^{-11}\ \mathrm{m/s}$ are identical, and the stress–strain curves for the cases of the drained condition and $\mathrm{k} = 10^{-7}\ \mathrm{m/s}$ are identical. This indicates that consolidation must be considered when the permeability coefficient is between $10^{-10}\ \mathrm{m/s}$ and $10^{-8}\ \mathrm{m/s}$.

Figure 11. Cavity expansion curve using consolidation analysis

The above process was plotted in the form of Mohr's circles, as shown in Figure 12. For the case of $\mathrm{k} = 10^{-7}\ \mathrm{m/s}$, the mean effective stress increases sharply after the Mohr circle violates the tensile failure criteria, and hence shows a rapid increase in shear strength. For this reason, the cavity pressure for higher permeability can reach a higher value.

Figure 12. Mohr circles at the cavity wall using consolidation analysis

Figure 13 shows the stiffness constant and friction angle derived by interpreting the data from Ng (2009) when considering consolidation. It seems that the undrained assumption leads to overestimation of the soil stiffness and strength. When the permeability increases to about $10^{-7}\ \mathrm{m/s}$, the stiffness constant and friction angle reduce to about 6.3 MPa and 12.9°. The errors are about 21% and 35.5%, respectively. This study therefore concludes that consolidation is a crucial factor in the process of the pressuremeter test, especially for soils with medium permeability between $10^{-10}\ \mathrm{m/s}$ and $10^{-8}\ \mathrm{m/s}$. Without considering soil consolidation, the derived geomechanical parameters in undrained condition may be much higher than the real values. It is unfortunate that making this error in data interpretation leads to a unsafe design in geotechnical engineering projects.

Figure 13. Effect of the permeability coefficient on soil stiffness and strength

6 Conclusions

In this paper, a 1D finite element model was presented as a tool to derive in situ soil parameters, based on comparing pressuremeter test results with the expected soil responses from FE analysis. The numerical results perfectly matched the analytical solutions under both drained and undrained condition, which indicates that FEM is a valid and flexible method for interpreting pressuremeter test data. The 1D model reduced the total number of elements and hence saved computational time without losing accuracy.

Tensile fracturing is one of the most important processes in the pressuremeter test. Good agreement between the in situ test results and the numerical simulations was obtained. Cavity pressure in the tensile/shear analysis is lower than in conventional shear analysis, when equivalent stiffness and shear strengths are used. Hence, for cohesive soil, neglecting to consider tensile failure will lead to overestimation of the stiffness constant and friction angle.

Normally, pressuremeter testing in clay is considered as an undrained process, but in reality some consolidation occurs for the clay with medium permeability. When the permeability coefficient is lower than $10^{-11}\ \mathrm{m}/s$, the pressuremeter test is assumed to be under undrained conditions. When the permeability coefficient is between $10^{-8}\ \mathrm{m}/s$ and $10^{-10}\ \mathrm{m}/s$, consolidation has a large effect on the results. It seems that the undrained analysis leads to overestimation of the soil stiffness and strength. When the permeability increases to about $10^{-7}\ \mathrm{m}/s$, the test process is close to a drained condition, and the errors in the derived stiffness constant and friction angle are about 21% and 35.5%, respectively.

Acknowledgement

This research work is part of the Centre for Smart Infrastructure & Construction at University of Cambridge. We thank Professor Kenichi Soga, (UC Berkeley) for comments that greatly improved the research results.

References

Ajalloeian, R., & Yu, H. S. (1998). Chamber studies of the effects of pressuremeter geometry on test results in sand. Geotechnique, 48(5), 621-636.

Bolton, M. D., Sun, H. W., & Britto, A. M. (1993). Finite element analyses of bridge abutments on firm clay. Computers and Geotechnics, 15(4), 221-245.

Bolton, M. D., & Whittle, R. W. (1999). A non-linear elastic/perfectly plastic analysis for plane strain undrained expansion tests. Geotechnique, 49(1), 133-41.

Clarke, B. G. (1994). *Pressuremeters in geotechnical design*. CRC Press.

Cunha, R.P. (1994). Interpretation of self-boring pressuremeter test in sand. Ph.D. dissertation, University of British Columbia, Vancouver.

Cunha, R.P. 1996. A new cavity expansion model to simulate selfboring pressuremeter tests in sand. Brazilian Geotechnical Journal (Solos e Rochas), 19(1): 15–27.

Emami, M., & Yasrobi, S. S. (2014). Modeling and Interpretation of Pressuremeter Test Results with Artificial Neural Networks. *Geotechnical and Geological Engineering*, *32*(2), 375-389.

Gibson, R. E., & Anderson, W. F. (1961). In situ measurement of soil properties with the pressuremeter. Civil engineering and public works review,56(658), 615-618.

Gunn, M. J. (1992). The prediction of surface settlement profiles due to tunnelling. Predictive soil mechanics, Proceedings of the Wroth Memorial Symposium, Oxford, pp. 304-316.

Houlsby, G. T., & Withers, N. J. (1988). Analysis of the cone pressuremeter test in clay. Geotechnique, 38(4), 575-587.

Houlsby, G. T., & Carter, J. P. (1993). The effects of pressuremeter geometry on the results of tests in clay. *Geotechnique*, *43*(4), 567-576.

Hughes, J. M. O., Wroth, C. P., & Windle, D. (1977). Pressuremeter tests in sands. Geotechnique, 27(4), 455-477.

Isik, N. S., Ulusay, R., & Doyuran, V. (2015). Comparison of undrained shear strength by pressuremeter and other tests, and numerical assessment of the effect of finite probe length in pressuremeter tests. Bulletin of Engineering Geology and the Environment, 74(3), 685-695.

Jefferies, M. G. (1988). Determination of horizontal geostatic stress in clay with self-bored pressuremeter. Canadian Geotechnical Journal, 25(3), 559-573.

Joshi, K., Ng, M. Y. A., & Soga, K. (2008). Mechanical behaviour of 11 years old contaminated cement-bentonite material. *DEFORMATION CHARACTERISTICS OF GEOMATERIALS, VOLS 1 AND 2*, 311-317.

Mitchell, J.K. and Soga, K. (2005). Fundamentals of soil behaviour. 3rd edition, John Wiley & Sons, Inc.

Mo, P. Q., Marshall, A. M., & Yu, H. S. (2014). Elastic- plastic solutions for expanding cavities embedded in two different cohesive- frictional materials. International Journal for Numerical and Analytical Methods in Geomechanics,38(9), 961-977.

Ng, M. Y. A. (2009). Modelling of hydraulic fracturing in cement bentonite geomaterials. Ph.D.

dissertation, University of Cambridge.

Sánchez, F. E., Aguado, M. B., & Lavín, J. R. S. (2014). Interpretation of the pressuremeter test using numerical models based on deformation tensor equations. Bulletin of Engineering Geology and the Environment, 73(1), 141-146.

Schnaid, F., Ortigao, J. A., Mantaras, F. M., Cunha, R. P., & MacGregor, I. (2000). Analysis of self-boring pressuremeter (SBPM) and Marchetti dilatometer (DMT) tests in granite saprolites. Canadian geotechnical journal, 37(4), 796-810.

Withers, N. J., Howie, J., Hughes, J. M. O., & Robinson, P. K. (1989). Performance and analysis of cone pressuremeter tests in sands.Geotechnique, 39(3), 433-454.

Wroth, C. P. (1982, April). British experience with the self-boring pressuremeter. In *Proc. of Int. Symp. Pressuremeter and its Marine Applications, Paris. Chapman & Hall, London* (pp. 143-164).

Yeung SK, Carter JP (1990) Interpretation of the pressuremeter test in clay allowing for membrane end effects and material non-homogeneity. Pressuremeters, proceedings of the symposium on pressuremeters, British Geotechnical Society, pp 199–208

Yu, H. S., & Houlsby, G. T. (1991). Finite cavity expansion in dilatant soils: loading analysis. *Geotechnique*, *41*(2), 173-183.

Yu, H. S. (2000). Finite Element Solutions. In Cavity Expansion Methods in Geomechanics (pp. 190-208). Springer Netherlands.

Figure captions

Figure 1. Sketch of the numerical model to simulate a pressuremeter test
Figure 2. Soil stress and pore flow velocity in axisymmetric problem
Figure 3. Mechanisms of tensile fracturing in undrained conditions (after Mitchell and Soga, 2005)
Figure 4. (a) complete yield surface (b) softening law of tensile strength
Figure 5. Cavity expansion curve from numerical drained analysis and analytical solution
Figure 6. Cavity expansion curve from numerical undrained analysis and analytical solution
Figure 7. Cavity expansion curve for shear and tensile/shear analysis
Figure 8. Stress path at the cavity wall
Figure 9. Mohr's circles at the cavity wall: (a) shear analysis ($\alpha = 8$Mpa); (b) tensile/shear analysis ($\alpha = 6.5$Mpa); (c) tensile/shear analysis ($\alpha = 8$Mpa)
Figure 10. Effect of tensile strength on soil stiffness and strength
Figure 11. Cavity expansion curve using consolidation analysis
Figure 12. Mohr circles at the cavity wall using consolidation analysis

Figure 13. Effect of the permeability coefficient on soil stiffness and strength

Table captions

Table 1 Soil parameters for drained/undrained analysis

Table 2 Soil parameters for shear and tensile/shear analysis

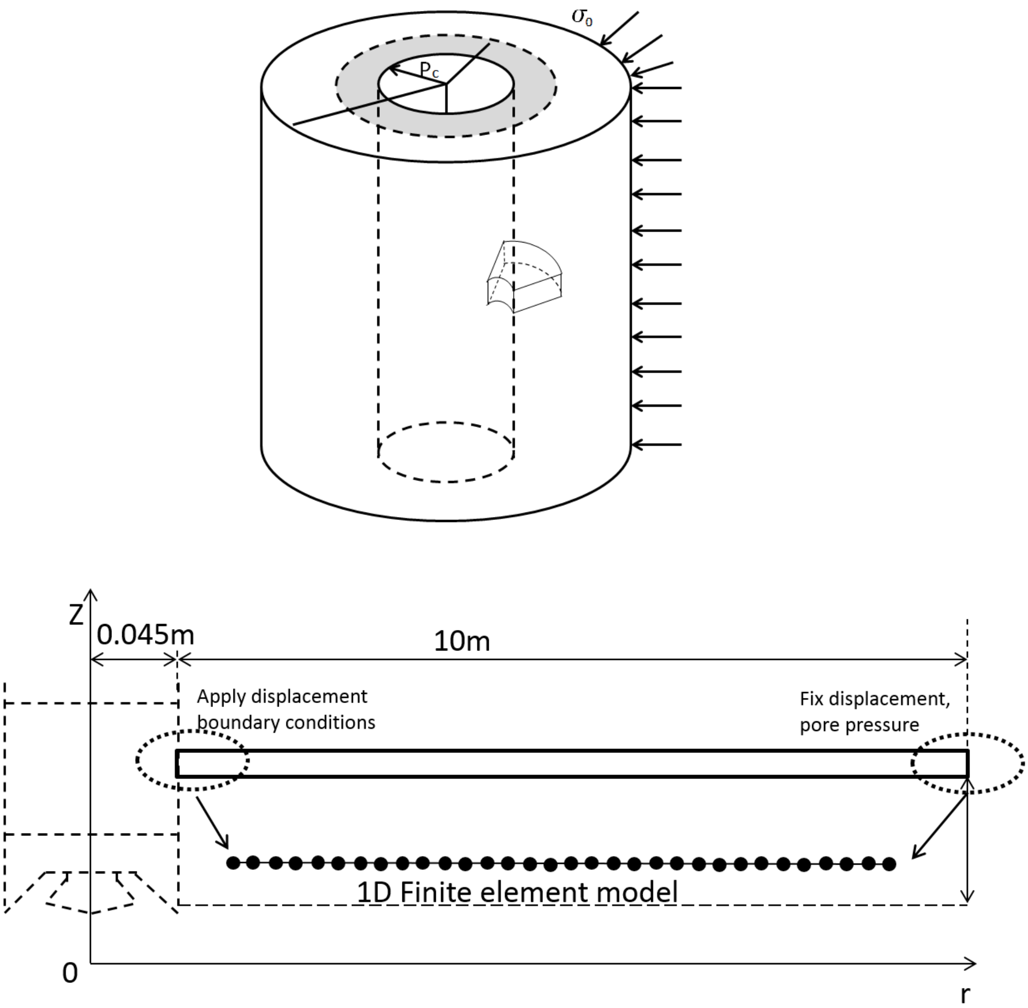

Figure 1. Sketch of the numerical model to simulate a pressuremeter test

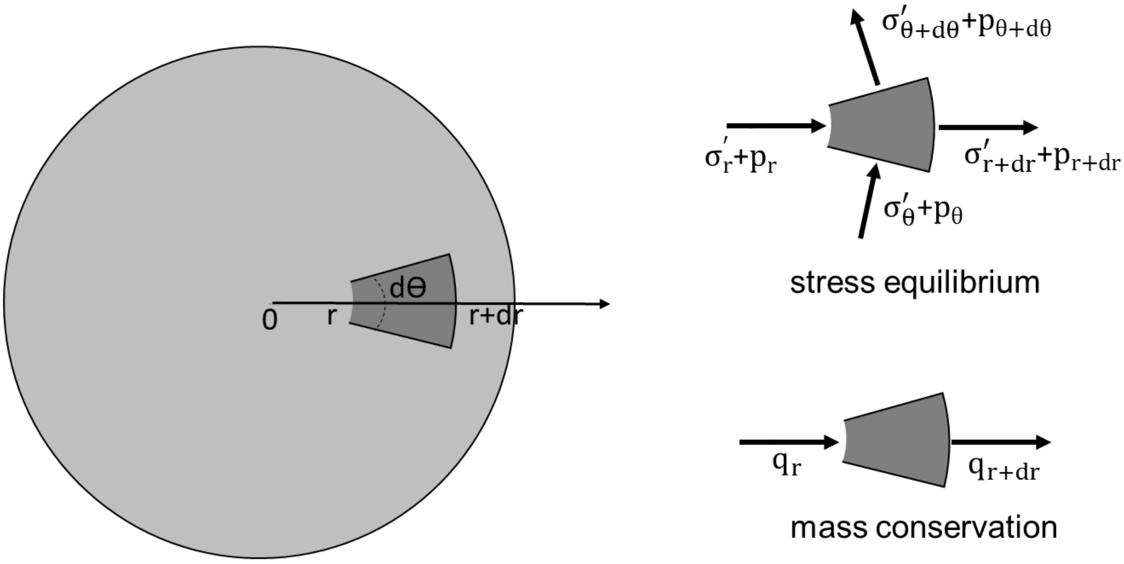

Figure 2. Soil stress and pore flow velocity in axisymmetric problem

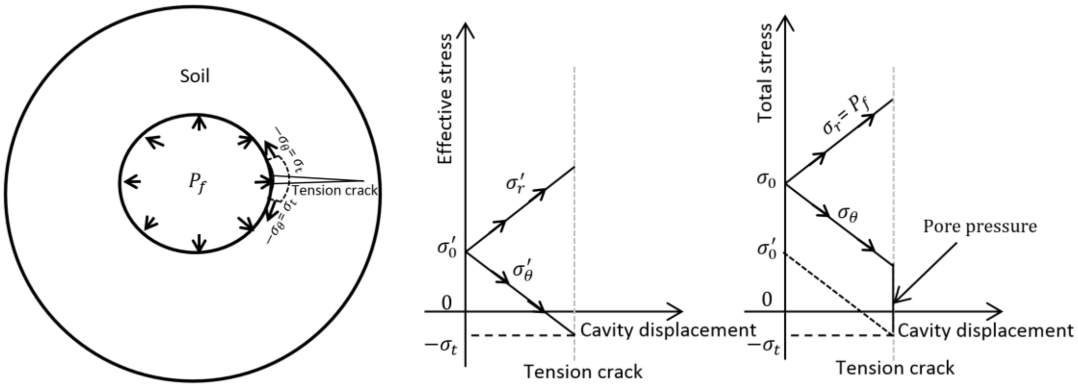

Figure 3. Mechanisms of tensile fracturing in undrained conditions (after Mitchell and Soga, 2005)

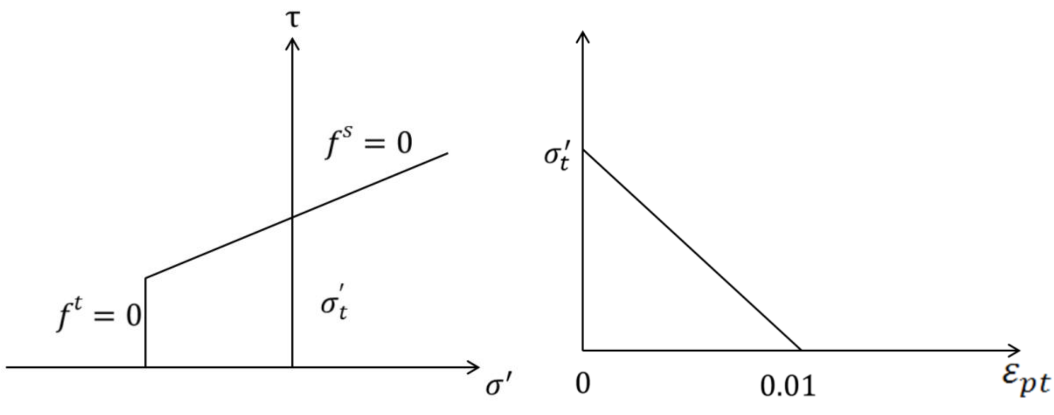

(a) (b)

Figure 4. (a) complete yield surface (b) softening law of tensile strength

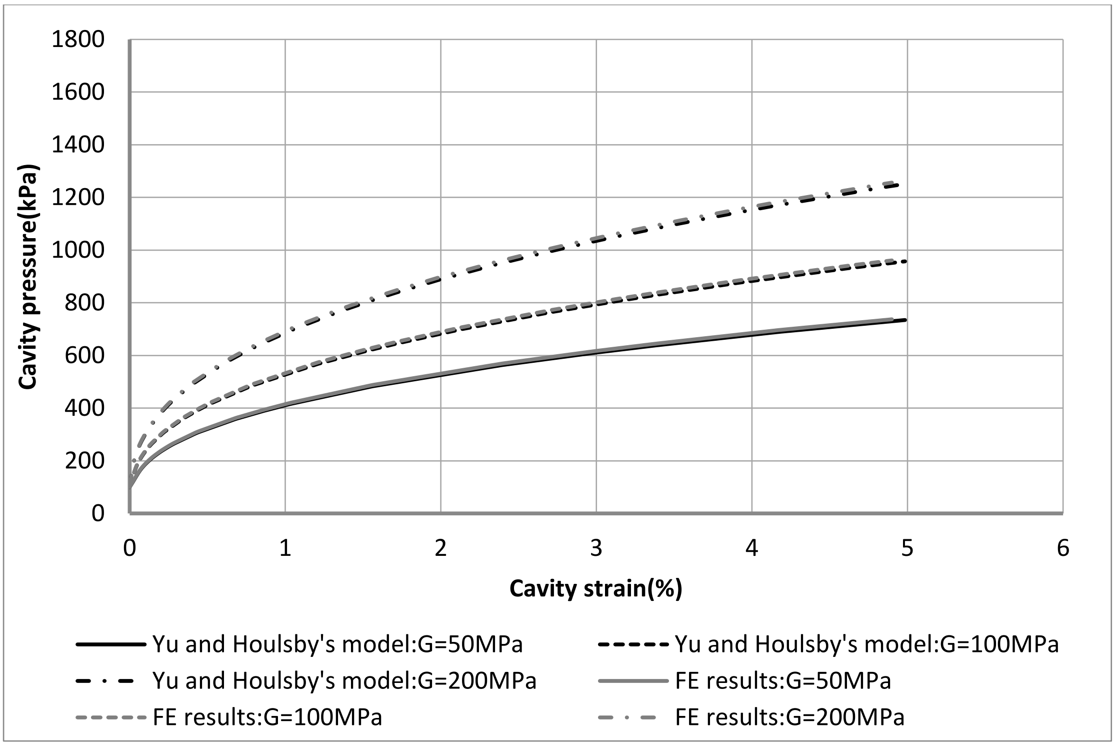

Figure 5. Cavity expansion curve from numerical drained analysis and analytical solution

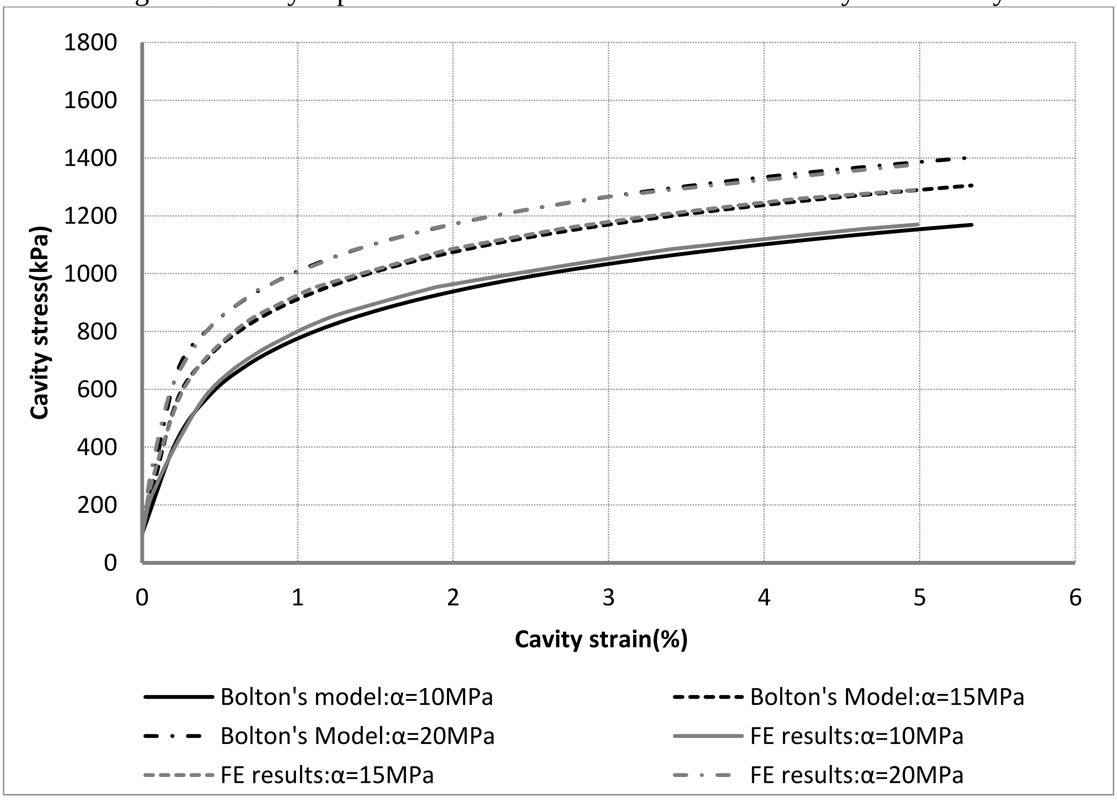

Figure 6. Cavity expansion curve from numerical undrained analysis and analytical solution

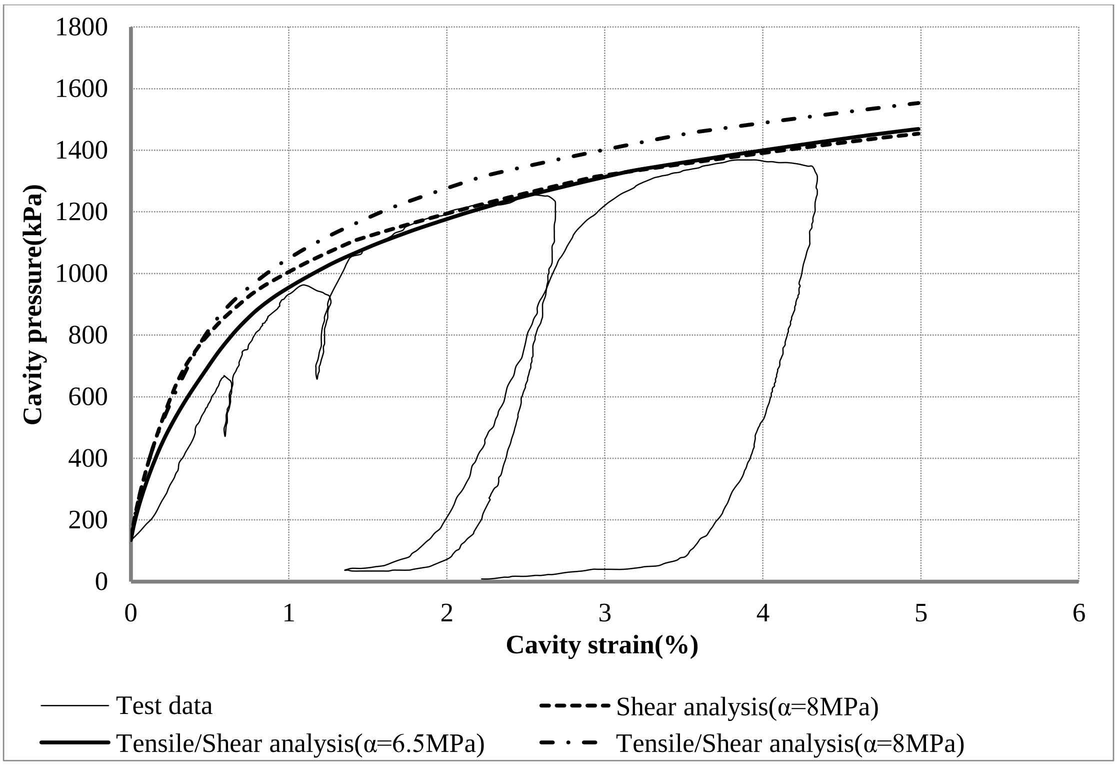

Figure 7. Cavity expansion curve for shear and tensile/shear analysis

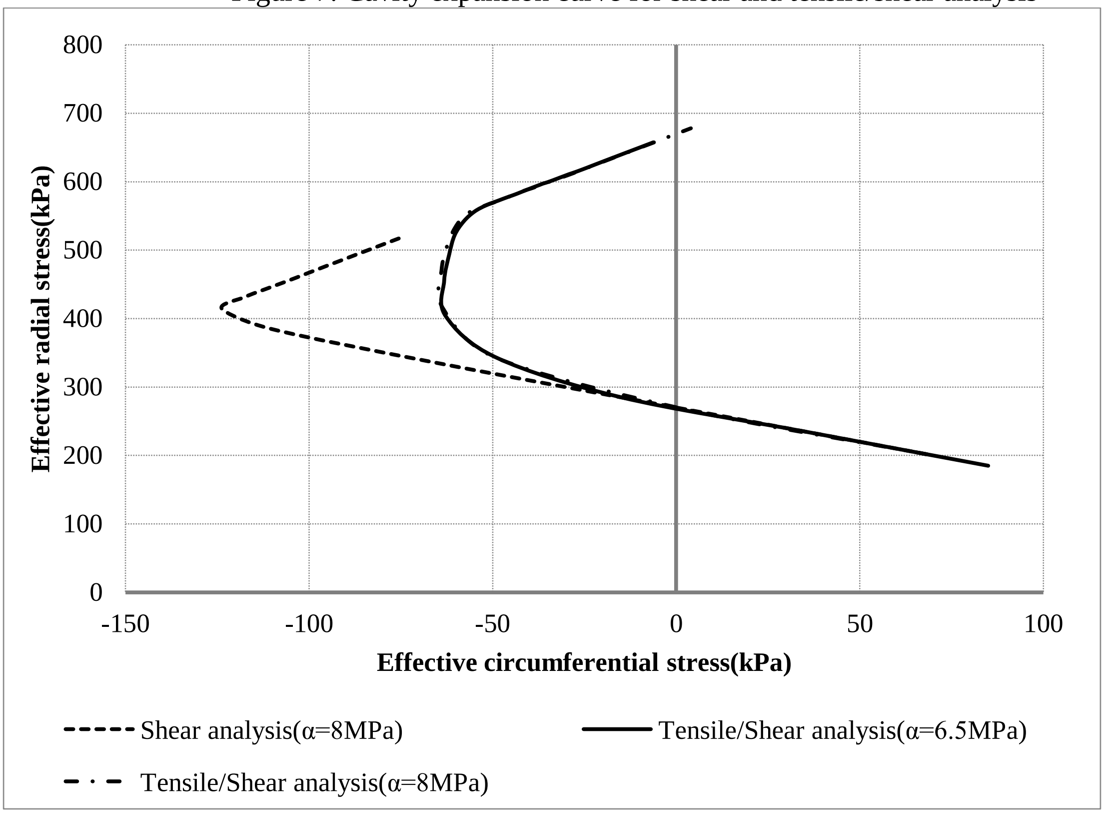

Figure 8. Stress path at the cavity wall

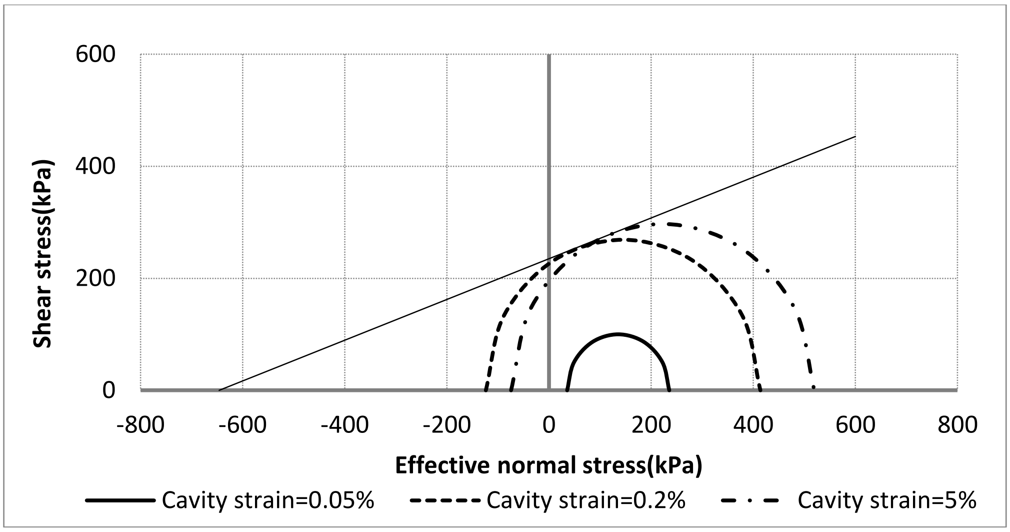

(a)

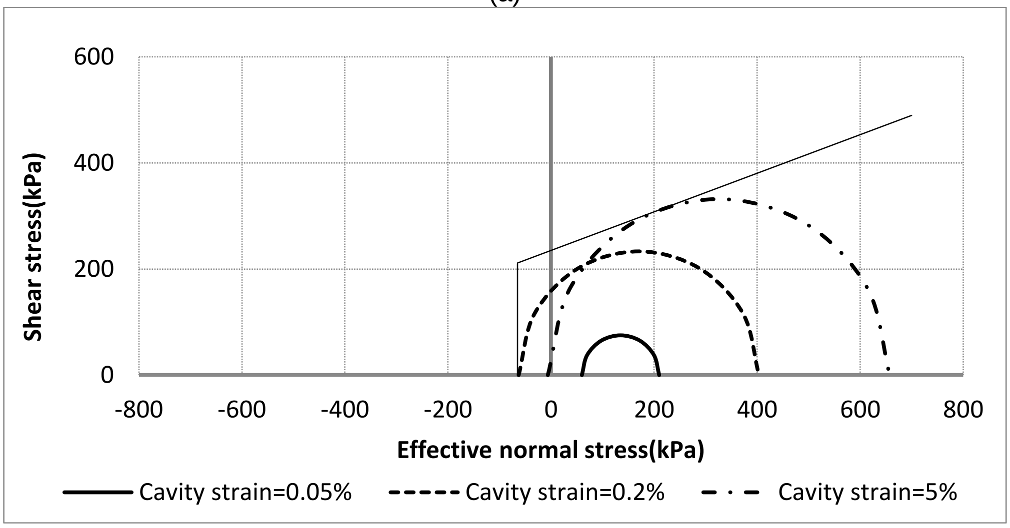

(b)

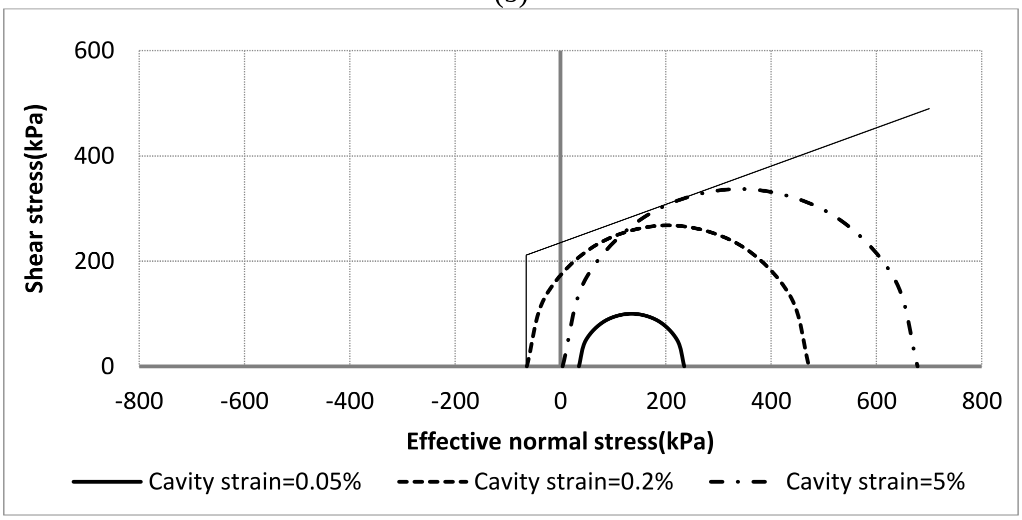

(c)

Figure 9. Mohr's circles at the cavity wall: (a) shear analysis ($\alpha = 8$MPa); (b) tensile/shear analysis ($\alpha = 6.5$MPa); (c) tensile/shear analysis ($\alpha = 8$MPa)

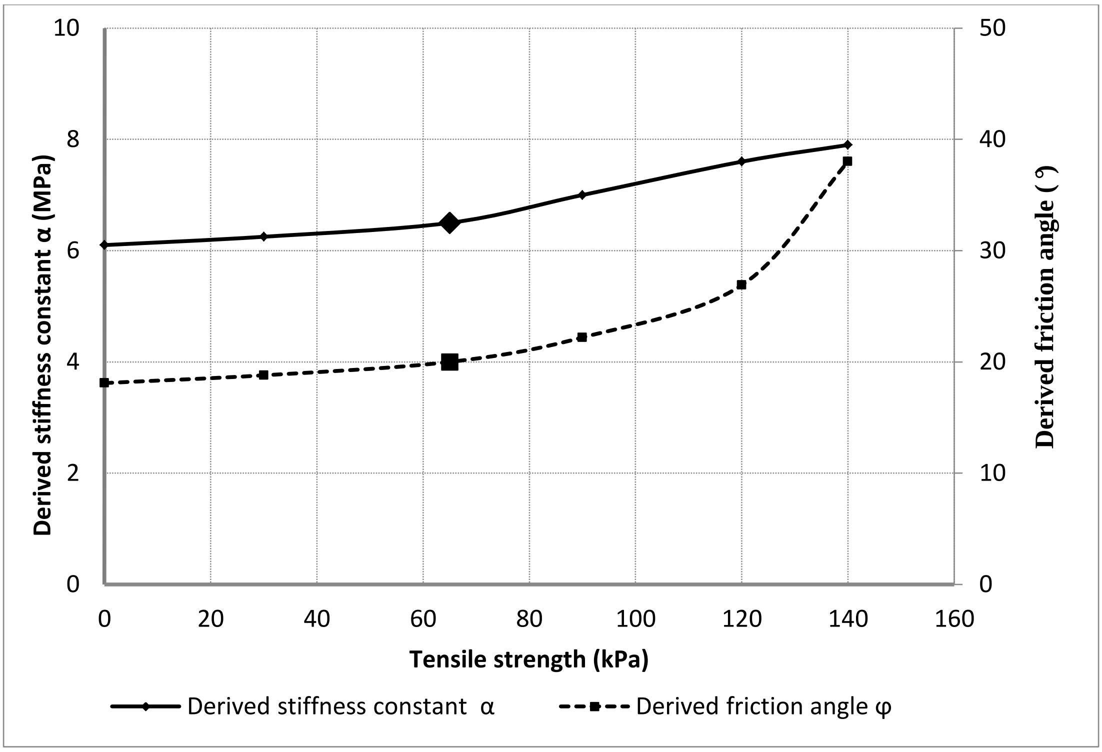

Figure 10. Effect of tensile strength on soil stiffness and strength

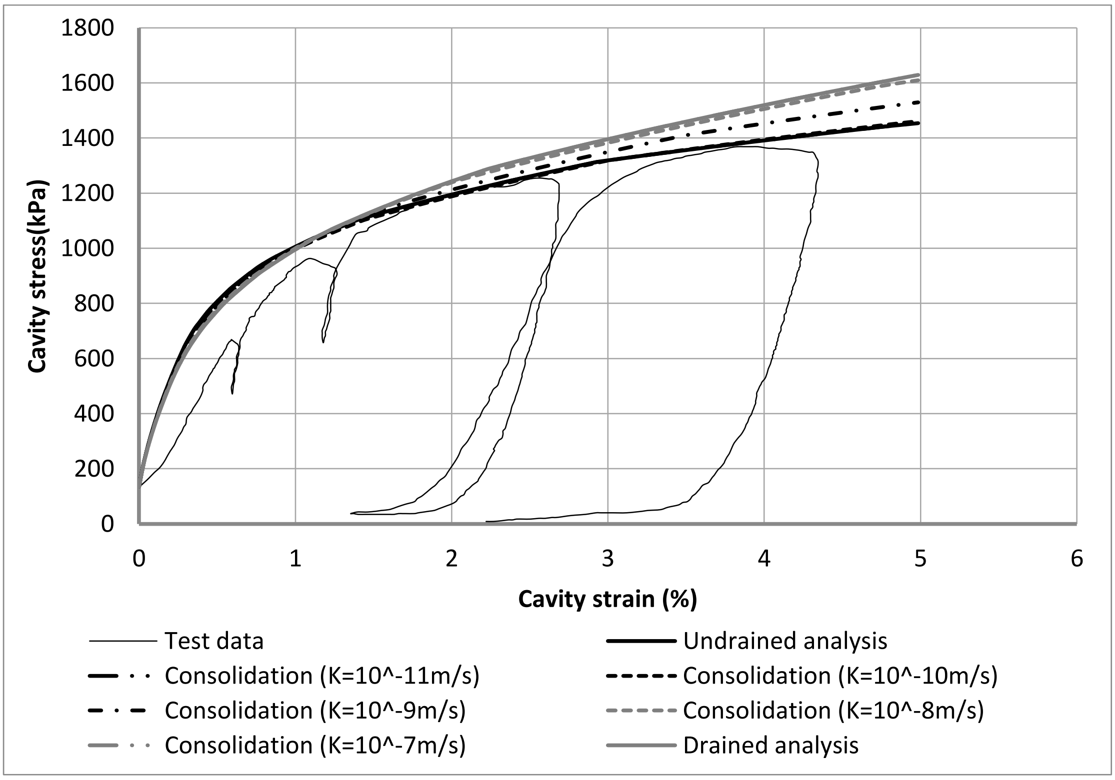

Figure 11. Cavity expansion curve using consolidation analysis

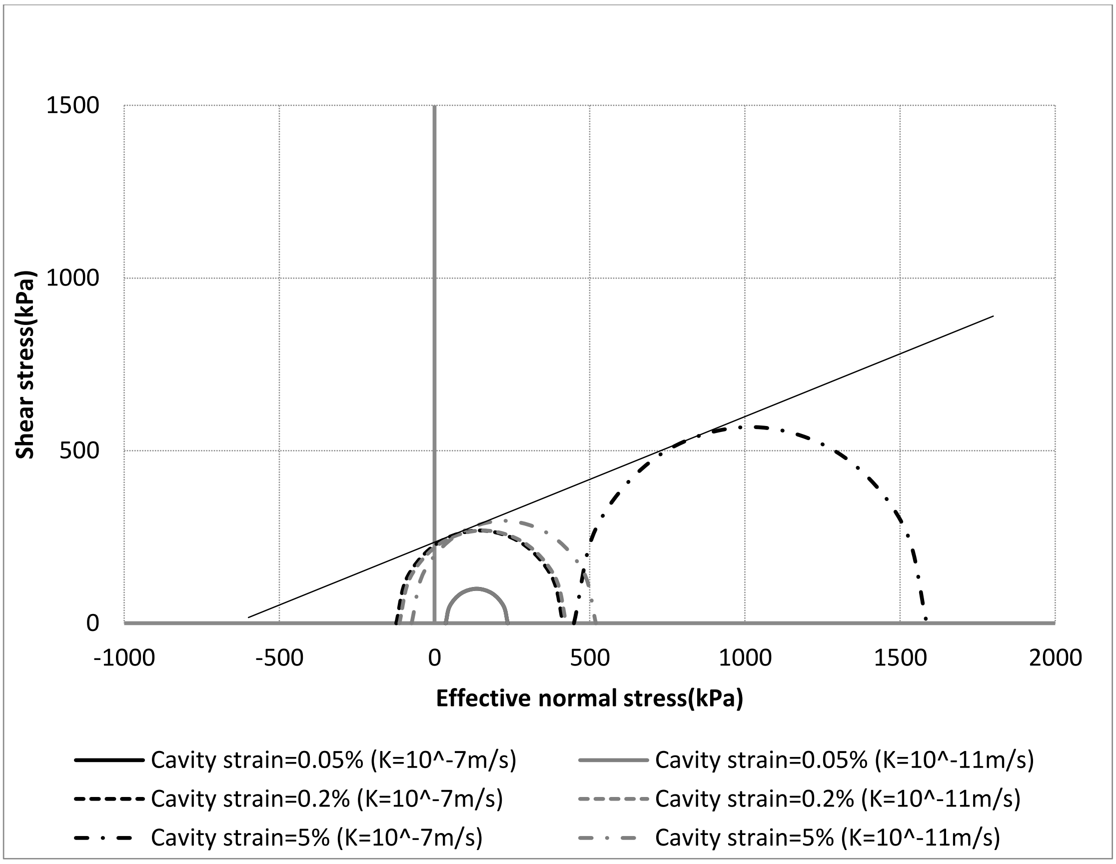

Figure 12. Mohr circles at the cavity wall using consolidation analysis

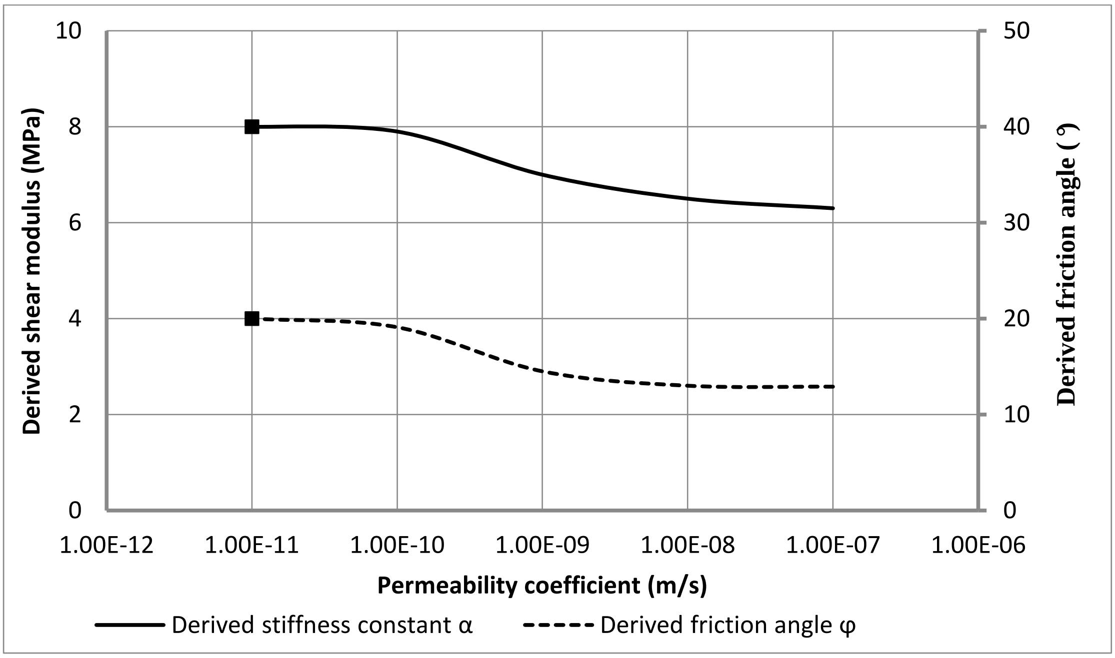

Figure 13. Effect of the permeability coefficient on soil stiffness and strength